# Lysozyme orientation and conformation on $MoS_2$ surface: Insights from molecular simulations

Hongjie Fan, Daohui Zhao, Yingtu Li, and Jian Zhou

Citation: Biointerphases **12**, 02D416 (2017); doi: 10.1116/1.4984803
View online: http://dx.doi.org/10.1116/1.4984803
View Table of Contents: http://avs.scitation.org/toc/bip/12/2
Published by the American Vacuum Society



# Lysozyme orientation and conformation on $MoS_2$ surface: Insights from molecular simulations

Hongjie Fan, Daohui Zhao, Yingtu Li, and Jian Zhou[a)]
*Guangdong Provincial Key Lab for Green Chemical Product Technology, School of Chemistry and Chemical Engineering, South China University of Technology, Guangzhou, Guangdong 510640, People's Republic of China*

(Received 24 February 2017; accepted 19 May 2017; published 2 June 2017)

Two-dimensional molybdenum disulfide ($MoS_2$) has attracted intense interest owing to its unique properties and promising biosensor applications. To develop effective biocompatible platforms, it is crucial to understand the interactions between $MoS_2$ and biological molecules such as proteins, but little knowledge exists on the orientation and conformation of proteins on the $MoS_2$ surface at the molecular level. In this work, the lysozyme adsorption on the $MoS_2$ surface was studied by molecular dynamics simulations, wherein six different orientations were selected based on the different faces of lysozyme. Simulation results showed that lysozyme tends to adsorb on the $MoS_2$ surface in an "end-on" orientation, indicating that orientations within this range are favorable for stable adsorption. The end-on orientation could be further categorized into "bottom end-on" and "top end-on" orientations. The driving forces responsible for the adsorption were dominated by van der Waals interactions and supplemented by electrostatic interactions. Further, the conformations of the lysozyme adsorbed on the $MoS_2$ surface were basically preserved. This simulation study promotes the fundamental understanding of interactions between $MoS_2$ and proteins and can guide the development of future biomedical applications of $MoS_2$. © *2017 American Vacuum Society*. [http://dx.doi.org/10.1116/1.4984803]

## I. INTRODUCTION

Since the discovery of graphene,[1] its compelling properties[2] and successful applications have opened the gate for two-dimensional (2D) layered materials. Another important 2D layered material that has been the focus of recent research is molybdenum disulfide ($MoS_2$), which belongs to the family of layered transition metal dichalcogenides with a formula $MX_2$. Further, $MX_2$ has a layered structure *X–M–X*, wherein a plane (*M*) of a transition metal element of group IV (Ti, Zr, and Hf), group V (V, Nb, and Ta), or group VI (Mo and W) is sandwiched between two hexagonal planes (*X*) of a chalcogenide (S, Se, and Te).[3,4] Single-layer $MoS_2$ exhibits some novel properties that are distinctly different from those of graphene. For example, single-layer $MoS_2$ possesses a direct bandgap[5] of 1.8 eV, while graphene has no bandgap. In addition, intrinsic 2D $MoS_2$ has a relatively lower toxicity than graphene.[6]

Further, $MoS_2$ possesses some promising applications in fields such as electronics, optoelectronics, energy storage, and sensors.[3,7–9] In particular, $MoS_2$ has great potential in the field of biosensors for the detection of biological molecules such as proteins.[10–12] An ultrasensitive and protein-specific biosensor[10] based on $MoS_2$ has been achieved with a sensitivity of 196 (defined as the ratio of the difference in current before and after biomolecule binding to the lower of the two currents) even at a concentration of 100 fM, which surpassed the sensitivity of a sensor based on graphene by more than 74-fold. An $MoS_2$ nanosheet-based field-effect device with versatile $HfO_2$-silane-based bio-functionalization was realized for label-free real-time detection of the cancer marker protein prostate-specific antigen.[11] An opioid biosensor based on $MoS_2$ field effect transistors[12] has been fabricated to couple a computationally redesigned variant of the $\mu$-opioid receptor.

It is of great importance in the development of these promising applications that the interactions between proteins and $MoS_2$ be understood. Experimentally, it is difficult to understand the adsorption dynamics at the picosecond scale or to study the surface morphology at the nanoscale level. As an alternative approach however, the molecular simulation has been adopted to investigate protein adsorption on nanomaterial surfaces,[13–15] and molecular dynamics (MD) is one such method that provides atomistic-level explanations of protein–surface interactions. Some attempts[16–19] have been made to explore biomolecule adsorption upon $MoS_2$ by means of MD simulations. Gu *et al.*[16] have studied the interaction between $MoS_2$ and $\alpha$-helices in polyalanine of various lengths, and their results showed that $MoS_2$ bound all peptides in a rapid and strong manner and induced drastic disruptions to the peptide structures. They[17] have also investigated the interaction of a $MoS_2$ nanotube with a $\beta$-sheet YAP65 WW domain and found that the adsorption of YAP65 on the $MoS_2$ nanotube lost most of the secondary and tertiary structures of the $\beta$-sheet domain. Gu *et al.*[18] have also explored the interaction of $\alpha$-helices of protein Villin Headpiece (HP35) with $MoS_2$ and observed a similar exceptionally robust denaturation capability of $MoS_2$ to HP35. All these works employed the $MoS_2$ force field developed by Varshney *et al.*[20] and exhibited a similar dramatic denaturation capacity of $MoS_2$ to peptides. Therefore, Luan and Zhou[21] believed that the force-field parameters in the study

[a)]Electronic mail: jianzhou@scut.edu.cn

by Varshney *et al.*[20] were too attractive and performed a new optimization that could accurately yield the experimentally measured contact angle (97.8°) of water on the $MoS_2$ surface.[22] Based on the $MoS_2$ force field reported by Luan and Zhou,[21] Gu *et al.*[19] have further examined the adsorption of the above three peptides on $MoS_2$ and compared the results by different force fields, which confirmed that the Luan force field more reasonably represents the interactions of $MoS_2$ with water and/or proteins. These works[16–19] have mainly focused on the denaturation ability of $MoS_2$ to peptides that possess typical and single secondary structures, but the orientations and conformations of larger proteins adsorbed on $MoS_2$ have not yet been investigated. It is crucial to explore protein–surface interactions via the analysis of the orientations and conformations attempted by previous numerous studies.[23–27] Herein, we chose lysozyme, a relatively large and structure-complete model protein, to study protein adsorption on $MoS_2$.

Lysozyme has been widely used to explore the interaction between solid materials and proteins. Kubiak-Ossowska and Mulheran[28] have performed classical MD simulations of lysozyme on a simplified mica surface model and found that the main adsorption site was located on the N,C-terminal part of the protein surface and that the major role was played by the residues Lys1, Arg5, Arg14, and Arg128. Raffaini and Ganazzoli[29] have probed the adsorption of human lysozyme with ten initial orientations on hydrophobic graphite through molecular mechanics and MD techniques. Wei *et al.*[30] have presented a series of MD simulations to study the orientation-dependent adsorption of lysozyme on a polyethylene surface. Their results suggested a faster adsorption for an "end-on" orientation but an ultimately more stable adsorption for a "side-on" orientation. Xie *et al.*[31] have applied the parallel tempering Monte Carlo method to simulate lysozyme orientations on charged surfaces and have demonstrated that the lysozyme tends to be adsorbed with a side-on orientation on negatively charged surfaces and that it could be adsorbed on positively charged surfaces with either an end-on or "back-on" orientation. Hildebrand *et al.*[32] have performed MD simulations to probe the adsorption of α-chymotrypsin and lysozyme on amorphous silica in comparison with adsorption experiments and found that lysozyme approaches the surface with a side-on orientation. Yu *et al.*[33] have adopted mesoscopic coarse-grained simulations to investigate the interfacial mechanisms via hydrophobic charge-induction chromatography (HCIC) for protein purification by regulating the *p*H. Simulation results indicated that the lysozyme adsorbs on a hydrophobic surface mainly with an end-on orientation.

In summary, lysozyme adsorption has been studied on some solid surfaces, but not yet on the $MoS_2$ surface. In this work, we attempt to understand the underlying interaction mechanisms of lysozyme adsorption on the $MoS_2$ surface by MD simulations. Six different initial orientations were selected by directing the six faces of lysozyme to the surface. The adsorption orientation and conformational change of the lysozyme on the $MoS_2$ surface will be discussed in detail. The driving forces for lysozyme adsorption on the $MoS_2$ surface as predicted by these simulations will be addressed.

## II. METHODS

### A. Proteins and surface models

The lysozyme[34] used in the simulations herein was taken from the Protein Data Bank (1HEL), and its structure is displayed in Fig. 1(a). It contained 129 residues, which could be categorized as α (residues 1–35 and 85–129) and β (residues 36–84) domains.[35] The α domain consisted of four α helices and a short $3_{10}$ helix; while the β domain comprised a triple-stranded antiparallel β sheet, a long loop, and a $3_{10}$ helix. It was an ellipsoidal protein with dimensions of about $3.5 \times 4.6 \times 3.5\,nm^3$ and had a molecular weight of about 15 kDa.[34] The protein was studied at *p*H 7, with lysine and arginine residues together with the N-terminus being protonated while aspartic acid and glutamic acid residues together with the C-terminus being deprotonated.[26] The protein consisted of 1960 atoms and bore eight positive net charges. The hydrophobicity and the electrostatic surfaces of the lysozyme as visualized by Chimera[36] are presented in Figs. 1(b) and 1(c), respectively. The potential parameters for the lysozyme were taken from the CHARMM27 (Ref. 37) force field.

The $MoS_2$ surface was modeled with an orthorhombic unit cell similar to that in the previous work by Varshney *et al.*,[20] and the surface contained 1794 atoms with dimensions of

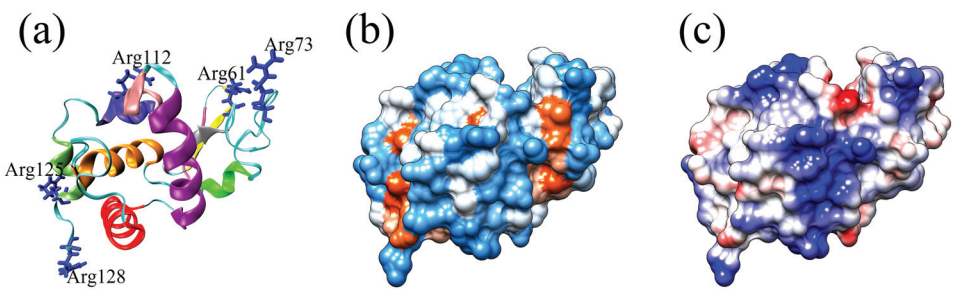


FIG. 1. Illustration of the lysozyme structures. (a) Secondary structure of the lysozyme (α domain: α-helix A (red); α-helix B (orange); α-helix C (purple); α-helix D (violet); $3_{10}$ helix (lime). β domain: β sheet 1 (mauve); β sheet 2 (yellow); β sheet 3 (silver); $3_{10}$ helix (green). Several arginine (Arg) residues (blue) are also labeled). (b) Hydrophobicity surface of the lysozyme [most hydrophilic (light blue), neutral (white), and most hydrophobic (orange)]. (c) Electrostatic surface of the lysozyme [negative (red), neutral (white), and positive (blue)].

TABLE I. Force field parameters for $MoS_2$.

| Atom | $\sigma$ (nm) | $\varepsilon$ (kJ/mol) | Charge (e) |
|---|---|---|---|
| Mo | 0.255 | 0.543 | 0.76 |
| S | 0.350 | 1.045 | −0.38 |

$7.268 \times 7.116\,nm^2$. The force field parameters employed for $MoS_2$, including partial charges and Lennard-Jones parameters $\varepsilon$ (the depth of the potential well) and $\sigma$ (the finite distance at which the interparticle potential is zero) for Mo and S atoms, were adopted from the study by Luan and Zhou[21] (see Table I). This $MoS_2$ force field was capable of reproducing the experimentally determined contact angle of water on the $MoS_2$ nanosheet and was used to study the interactions between $MoS_2$ and lysozyme.

### B. MD simulations

Six different faces of the lysozyme were directed to the $MoS_2$ surface to obtain six different initial orientations, which were selected as the starting orientations for the MD simulations (Fig. 2). All simulations were performed using the TIP3P (Ref. 38) water model and the CHARMM27 protein force field[37] through the GROMACS 4.5.4 (Ref. 39) package. The lysozyme-$MoS_2$ system was solvated in a water box of $7.268 \times 7.116 \times 7.084\,nm^3$, wherein eight chloride ions were added to neutralize the system. The initial closest distance between the lysozyme and the $MoS_2$ surface was about 10 Å. Finally, simulation trajectories were visualized using the visual molecular dynamics program.[40]

The $MoS_2$ surface was kept fixed throughout the simulations. The simulations were performed in an isochoric-isothermal (NVT) ensemble with a time step of 2 fs, and the temperature was controlled using a Nose-Hoover thermostat[41] with a 0.5 ps coupling constant to maintain the system at 300 K. All hydrogen atoms were constrained by the LINCS algorithm,[42] and the nonbonded interactions were treated with a cut-off of 11 Å. The particle mesh Ewald treatment[43] was used to calculate electrostatic interactions. The entire MD run process was set as follows: first, the steepest descent method was used to remove any inappropriate geometry or steric overlap to ensure that the system was energy-minimized. Next, an NVT equilibration of 100 ps was performed with position restraints on the backbone atoms of the protein. Finally, each system underwent 100 ns MD simulation.

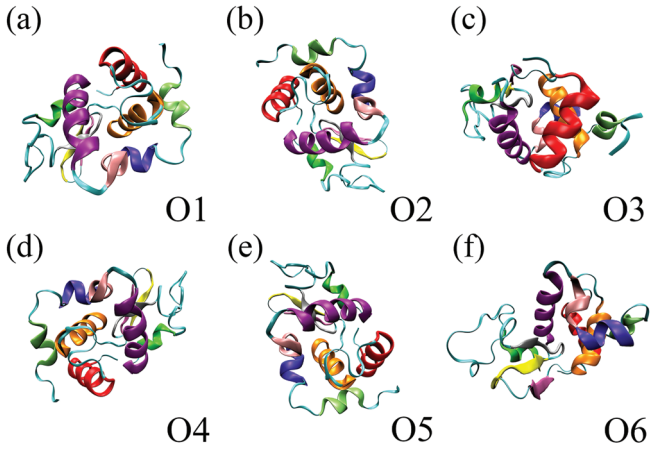


FIG. 2. Six initial orientations for lysozyme adsorption simulations.

## III. RESULTS AND DISCUSSION

Studying and understanding the underlying interaction mechanisms between the protein and the $MoS_2$ surface have a great significance for the development of new tailored applications in the field of biosensors, nanomedicine, and biochemistry. We investigated the lysozyme adsorption on an $MoS_2$ surface using MD simulations and also investigated the behavior of lysozyme in the bulk solution for comparison. In Secs. III A–III D, we first generally explain the orientation and interaction energies and then analyze the evolution of the key contact residues and their contribution to the adsorption. Finally, we discuss the overall conformational change of lysozyme and characterize the change by the root mean square fluctuation (RMSF), the root-mean-square deviation (RMSD), the radius of gyration ($R_g$), the eccentricity, the dipole moment, and secondary structures. Simulation results are shown in Tables II–III and Figs. 2–7.

### A. Adsorption orientation

Identification of the protein orientation is important for protein adsorption on material surfaces. We directed six different faces of the lysozyme onto the $MoS_2$ surface as the initial orientations for MD simulations (Fig. 2).

All six systems underwent 100 ns MD simulation to explore the adsorption behavior of lysozyme on the $MoS_2$ surface, where the six systems were marked as O1, O2, O3, O4, O5, and O6. The adsorption orientations after 100 ns simulation are shown in Fig. 3, and the orientation distributions are given in Fig. 4.

From Fig. 3, it can be clearly seen that, despite the different initial orientations, the adsorption orientations of lysozyme on the $MoS_2$ surface after 100 ns simulation tend to be the end-on orientation.[31,33] This indicates that the end-on orientation is favorable for a stable adsorption of lysozyme on the $MoS_2$ surface. Among the orientations, O1 and O5 form a "bottom end-on" orientation, while O2, O3, O4, and O6 form a "top end-on" orientation after reaching a stable adsorption. The results of the orientation distribution are

TABLE II. Orientation and interaction energies of lysozyme adsorbed on the $MoS_2$ surface.

| System | $\cos\theta$ | $U_{Ele}$ (kJ/mol) | $U_{vdW}$ (kJ/mol) | $U_{tot}$ (kJ/mol) |
|---|---|---|---|---|
| O1 | −0.85 ± 0.07 | −89.6 ± 18.0 | −242.2 ± 11.4 | −331.8 ± 22.7 |
| O2 | 0.74 ± 0.08 | − 62.1 ± 13.9 | −169.6 ± 8.7 | −231.7 ± 17.8 |
| O3 | 0.72 ± 0.09 | −135.2 ± 18.3 | −305.2 ± 12.4 | −440.4 ± 24.7 |
| O4 | 0.70 ± 0.11 | −159.1 ± 22.1 | −337.5 ± 19.5 | −496.6 ± 31.5 |
| O5 | −0.90 ± 0.10 | −104.9 ± 12.7 | −108.0 ± 8.5 | −212.9 ± 17.6 |
| O6 | 0.73 ± 0.11 | −162.1 ± 19.6 | −310.3 ± 27.6 | −472.4 ± 38.8 |

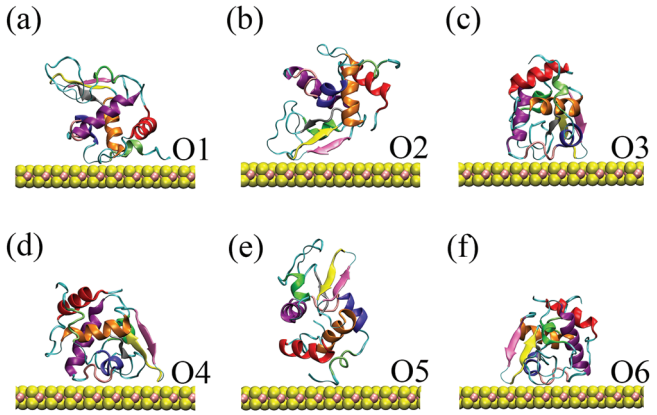


FIG. 3. Orientations of lysozyme adsorbed on the $MoS_2$ surface after 100 ns simulation. For clarity in the image, water and ions are not shown.

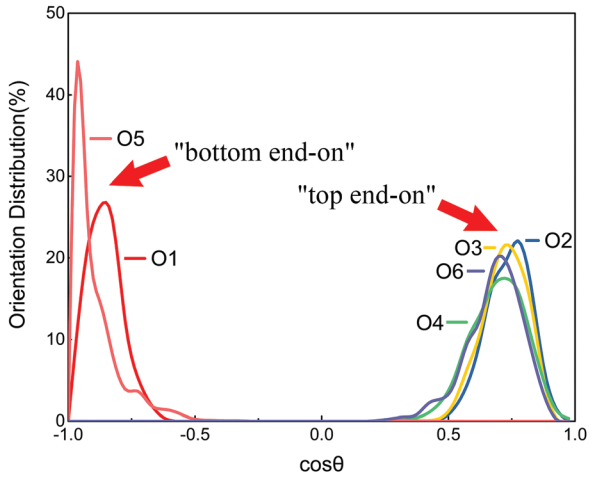


FIG. 4. Orientation distributions of the lysozyme dipole on the $MoS_2$ surface by MD simulations.

similar to those in the study by Yu *et al.*,[33] in which the adsorption orientations of lysozyme with HCIC tend to be an end-on orientation at *p*H 7. The $MoS_2$ surface is most likely a hydrophobic surface similar to the HCIC surface at *p*H 7. Experimental results[22] have given a wetting angle of water on a monolayer of $MoS_2$ of about 97.8°. Further, the simulation results in the study by Luan and Zhou[21] also suggest that the $MoS_2$ nanosheet is hydrophobic and has a low-friction surface. This infers that the adsorption of the lysozyme on the $MoS_2$ surface is driven by hydrophobic interactions, which will be further discussed through analysis of the interaction energy in Sec. III B.

Figure 4 shows the orientation distribution characterized by the cosine values of the orientation angles from the trajectories obtained during the last 20 ns simulation. The orientation angle ($\theta$) was defined as the angle between the surface normal and the protein dipole.[23,26,27,31] As can be seen in Fig. 4, the end-on orientation[33] is the dominant orientation for lysozyme adsorption on the $MoS_2$ surface. This end-on orientation can be further divided[33] into two classes: bottom end-on orientation ($\cos\theta < -0.6$) and top end-on orientation ($\cos\theta > 0.5$). Observing the data in Table II, we can see that

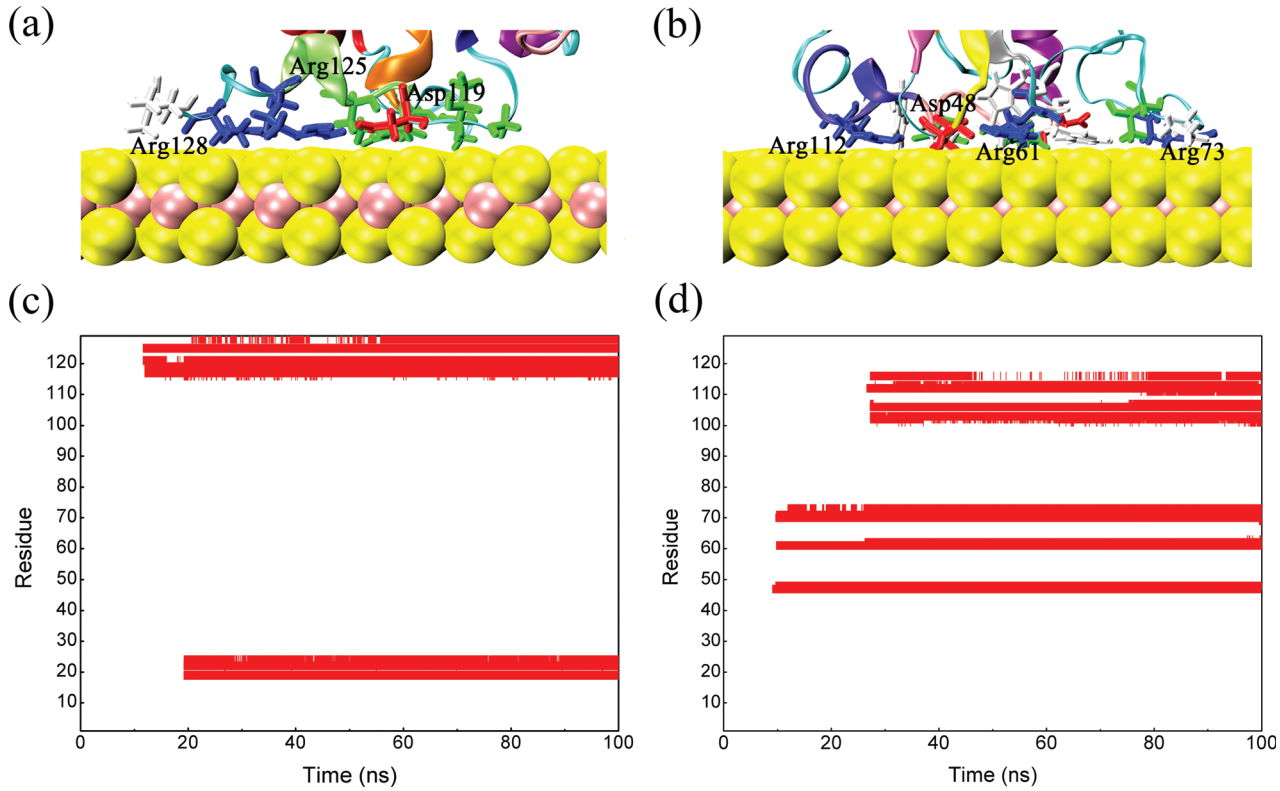


FIG. 5. Contact residue analysis of the key amino acids adsorbed on the $MoS_2$ surface with the typical configurations after the 100 ns simulation for the (a) bottom end-on orientation O1 and (b) top end-on orientation O4; and during the adsorption process for the (c) bottom end-on orientation O1 and (d) top end-on orientation O4. Key amino acids shown are positive (blue), negative (red), polar (green) and nonpolar (gray).

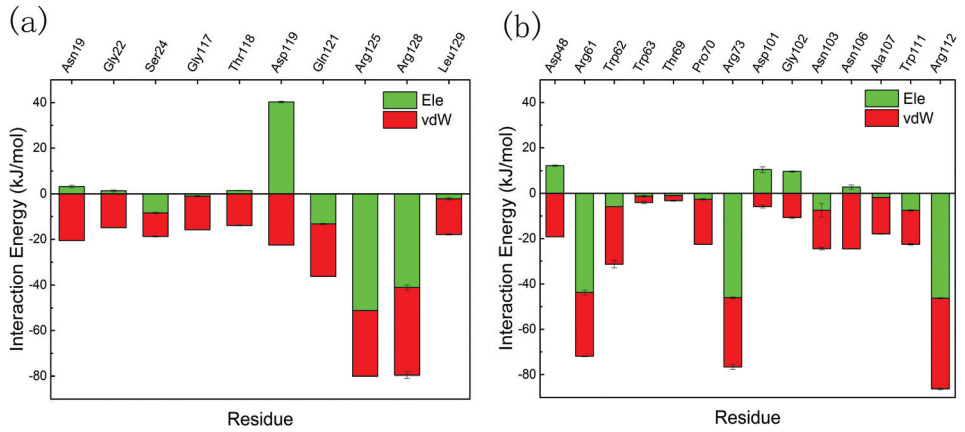


FIG. 6. Interaction energies of key adsorbed amino acids of lysozyme adsorbed on the $MoS_2$ surface for the two typical orientations of (a) bottom end-on orientation O1 and (b) top end-on orientation O4. The residue-based interaction energy includes electrostatic (Ele) and van der Waals (vdW) contributions.

O1 and O5 form bottom end-on orientations with averaged cosine values of −0.85 and −0.90, respectively; while O2, O3, O4, and O6 form top end-on orientations with averaged cosine values of 0.74, 0.72, 0.70, and 0.73, respectively. It is worth noting that O5 has a narrower orientation distribution than the others. This narrow distribution is mainly owing to the adsorption motif of lysozyme with $MoS_2$; the lysozyme adsorbed on the surface with a C-terminal and with other residues of Arg125, Gly126, Cys127, and Arg128, as can be seen in Fig. 3(e). It has been recognized that adjacent Arg125 and Arg128 enhance the adsorption of lysozyme, which leads to a relatively narrow distribution of the dipole angle.

## B. Interaction energy

To investigate the underlying adsorption mechanisms, it is necessary to further study the driving force for lysozyme adsorption on the $MoS_2$ surface. The averaged interaction energies between lysozyme and the $MoS_2$ surface for all systems were computed from the last 20 ns of MD trajectories,

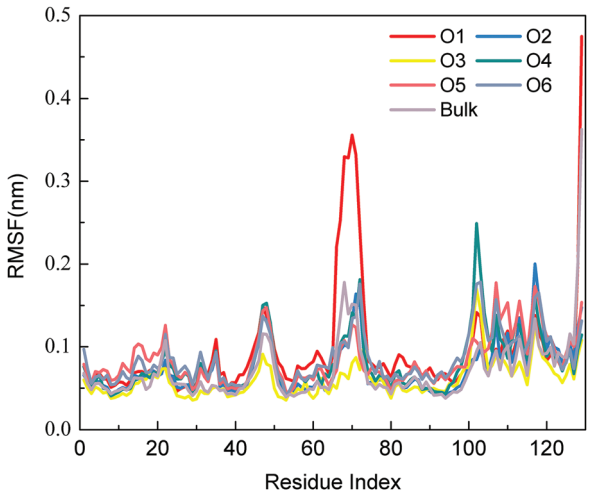


FIG. 7. RMSF values of backbone atoms per residue of the lysozyme in the bulk solution and on the $MoS_2$ surface.

which are shown in Table II. Herein, the total interaction energies include the averaged van der Waals (vdW) interaction energy ($U_{vdW}$) and electrostatic interaction energy ($U_{Ele}$) between lysozyme and the $MoS_2$ surface. Meanwhile, the total interaction energy ($U_{tot}$) was the sum of $U_{vdW}$ and $U_{Ele}$.[44]

It can be seen inTable II that all systems include both $U_{vdW}$ and $U_{Ele}$ contributions, regardless of the bottom end-on or top end-on orientations. Compared with the previous work by Yu *et al.*,[33] the $MoS_2$ and HCIC surfaces are both hydrophobic and the lysozyme tends to adsorb with similar orientations. However, the driving forces of lysozyme adsorbed on $MoS_2$ include both vdW and electrostatic interactions, while on HCIC, there is only vdW interaction. This may be ascribed to the intrinsic electron transfer[16] from Mo to S atoms, leading to a weak negatively charged outermost surface (S-sublayer) of $MoS_2$. In a recent work, Beckner *et al.*[45] have studied the lysozyme adsorption on oligo(ethylene glycol) (OEG) self-assembled monolayers (SAMs) and have shown that lysozyme was equally likely to be adsorbed on OEG SAMs exhibiting bottomwise adsorption with Arg68 and Arg44; sidewise adsorption with Arg14, Arg21, Ser86, and Arg112; and topwise adsorption with Arg125 and Arg128. The favored orientation results from the entropy gain of the solvent molecule release, attractive coulombic and vdW interactions, and hydrogen bonds. For each system, the $U_{vdW}$ energy is larger than the $U_{Ele}$ energy, indicating that both vdW and electrostatic interactions have contributions to the adsorption of lysozyme on the $MoS_2$ surface, where the former plays a more vital role. The interaction energies between lysozyme and the $MoS_2$ surface indicate that the adsorption is mainly dominated by hydrophobic interactions. This is different from the result of lysozyme adsorbed on charged surfaces in a previous work by Xie *et al.*,[31] in which the adsorption of lysozyme on a negatively charged surface is dominated by electrostatic interactions and the adsorption orientations tend to be the side-on orientation. The magnitude of the relationship between $U_{vdW}$ and $U_{Ele}$ is consistent with previous works,[16–19] which explore the interactions between three different peptides and $MoS_2$.

For systems with the bottom end-on orientation, O1 has a lower total interaction energy, which may be ascribed to an increased number of binding sites (the number of adsorbed residues) that result in a larger contact between the protein and the surface. In contrast, O5 has fewer binding sites (only four residues; Arg125, Gly126, Cys127, and Arg128), as described before, leading to relatively weaker $U_{vdW}$ and $U_{tot}$. For systems with the top end-on orientation, O4 possesses the lowest total interaction energy, while O2 possesses the highest total interaction energy, as shown in Fig. 4.

### C. Key residue analysis

Because adsorption occurs between the surface and the amino acids near the surface, we further investigated the interaction energies between the key residues and the surface. Herein, the criterion of the key amino acids is defined as the closest distance between any atoms of the amino acid to the surface within 3.5 Å.[44] From Table II, we selected the O1 bottom end-on orientation and the O4 top end-on orientation as corresponding representative systems to further analyze the interactions between lysozyme and the $MoS_2$ surface. The contact residue analysis and interaction energies of the key residues adsorbed on the $MoS_2$ surface are illustrated in Figs. 5 and 6.

Figure 5 shows the key residues that come into contact with the surface after a period of reorientation and maintain the stable adsorption state until the end of the simulation. Figure 6 shows that all these key residues have $U_{vdW}$ elements with different magnitudes, and their vdW interactions with the $MoS_2$ surface are greater than the electrostatic interactions.

Figure 5(a) displays the key amino acids adsorbed on the $MoS_2$ surface for the O1 system. The key residues contain six polar amino acids (Asn19, Gly22, Ser24, Gly117, Thr118, and Gln121), one nonpolar amino acid (Leu129), two positively charged amino acids (Arg125 and Arg128), and one negatively charged amino acid (Asp119). As illustrated in Fig. 5(c), the initial contacts of these key residues for O1 take place within 20 ns except Leu129 and are adsorbed tightly on the surface until the end of the simulation. The diversity of the key residues can be explained using Fig. 6(a). Each uncharged residue has a larger $U_{vdW}$ than $U_{Ele}$. The positively charged residues Arg125 and Arg128 have a much larger $U_{Ele}$, which is favorable for adsorption, while the negatively charged residue Asp119 has repulsive $U_{Ele}$, which is unfavorable for adsorption but can be compensated by $U_{vdW}$. From Fig. 5(a), we can see that the side chains of Arg125 and Arg128 are nearly parallel to the surface, which increases the contact area and leads to enhanced vdW interactions and a stable adsorption of lysozyme on the $MoS_2$ surface. This phenomenon was also found in a previous study[44] regarding the adsorption of horse heart cytochrome c upon a bare gold surface. This also indicates that most of these residues are in contact with the surface via nonpolar aliphatic chains while the polar groups are pointing outward to the solution, revealing that the vdW interaction plays an important role in lysozyme adsorption on the $MoS_2$ surface.

Figure 5(a) presents the snapshots of the key amino acids and the $MoS_2$ surface after 100 ns simulation of the O4 system. The key residues contain four polar amino acids (Thr69, Gly102, Asn103, and Asn106), six nonpolar amino acids (Trp62, Trp63, Pro70, Gly71, Ala107, and Trp111), three positively charged residues (Arg61, Arg73, and Arg112), and two negatively charged residues (Asp48 and Asp101). As for O4, a similar analysis was obtained by combining Figs. 5(d) and 6(b), where it is found that O4 has more contact residues and faster adsorption than O1. Notably, three positively charged residues (Arg61, Arg73, and Arg112) are beneficial for the adsorption, which can be indicated by the adsorption motifs in Fig. 5(b) and the interaction energies in Fig. 6(b). Comparing Figs. 6(a) and 6(b), the sum of $U_{vdW}$ and $U_{Ele}$ for most key residues in the O4 system is larger than that in the O1 system, inducing a stronger interaction for lysozyme adsorption on the $MoS_2$ surface.

### D. Conformation stability

To determine the structural stability of lysozyme, the RMSF of backbone atoms per residue in the bulk solution and on the $MoS_2$ surface was calculated from the last 20 ns of MD trajectories, and the results are displayed in Fig. 7. To quantify the conformation changes of lysozyme during the adsorption process, the RMSD of the backbone atoms, and the $R_g$ value, the eccentricity, and the dipole moment of lysozyme were calculated and are summarized in Table III.

As seen in Fig. 7, the RMSF values of most residues of lysozyme in the bulk solution and on the $MoS_2$ surface are less than 2 Å, which indicates that the lysozyme is in a stable conformation. In the bulk solution, the C-terminal displays a relatively larger RMSF value. For the O1 system, the loop residues 66–72 and the C-terminal exhibit higher RMSF values than those in the bulk solution and those on the surfaces adsorbed with other orientations. For the O4 system, the loop residues 102–103 also have higher RMSF values. These results can explain why O1 and O4 possess higher RMSD values. As discussed above, the residues with higher RMSF values are mainly located in the loop and the C-terminal, which usually present higher flexibility and mobility. Similar larger fluctuations of the loop residues 66–72 and 102–103 have been found in a previous work.[46]

TABLE III. Averaged properties of lysozyme in bulk solutions and adsorbed on an $MoS_2$ surface.

| System | RMSD (Å) | $R_g$ (Å) | Eccentricity | Dipole (D) |
|---|---|---|---|---|
| Water | 1.37 ± 0.13 | 13.89 ± 0.07 | 0.138 ± 0.005 | 148.1 ± 35.2 |
| O1 | 1.60 ± 0.10 | 14.02 ± 0.07 | 0.151 ± 0.005 | 157.7 ± 24.8 |
| O2 | 1.42 ± 0.12 | 13.81 ± 0.05 | 0.139 ± 0.005 | 212.2 ± 21.9 |
| O3 | 1.41 ± 0.09 | 14.12 ± 0.07 | 0.163 ± 0.005 | 210.5 ± 21.5 |
| O4 | 1.42 ± 0.15 | 13.97 ± 0.08 | 0.138 ± 0.005 | 146.4 ± 22.0 |
| O5 | 1.50 ± 0.17 | 13.91 ± 0.11 | 0.137 ± 0.007 | 167.4 ± 29.0 |
| O6 | 1.61 ± 0.20 | 13.88 ± 0.15 | 0.135 ± 0.009 | 173.7 ± 36.6 |

The averaged properties with respect to conformational changes of the lysozyme in the bulk solution and on the $MoS_2$ surface as mentioned at the start of Sec. III are summarized in Table III. After adsorption, the backbone RMSD values fluctuate within the range of $1.41 \pm 0.09$ to $1.61 \pm 0.20$ Å, while the averaged RMSD value is $1.37 \pm 0.13$ in the bulk solution, suggesting that the structure of lysozyme is well preserved when adsorbed on the surface. The $R_g$ and eccentricity values are very close to those in water, indicating no significant overall conformational change of lysozyme after adsorption. The dipole moment values are larger than those in the water solution, indicating that lysozyme induces some structural rearrangement in the adsorption process. In addition, the values of $R_g$ (13.89 Å for bottom end-on orientation O1 and 13.97 Å for top end-on orientation O4) are between those in the two studies[29,47] on lysozyme adsorption on a graphite surface (about 17 Å for Ref. 29 and about 12 Å for Ref. 47). Further, the dipole moment values are close to those of a previous work[32] on lysozyme adsorbed on an amorphous silica surface with a dipole of 153.8 D.

## IV. CONCLUSIONS

In this work, we studied the adsorption of lysozyme on an $MoS_2$ surface with six different initial orientations by MD simulations. The simulation results show that lysozyme adsorbs on the surface with bottom end-on and top end-on orientations. These two categories can be further summarized as an end-on orientation, indicating that lysozyme tends to adsorb on the $MoS_2$ surface with this orientation. The driving forces for lysozyme adsorption on the surface contain van der Waals and electrostatic interactions, suggesting that both interactions contribute to the adsorption. The former plays the dominant role, while the latter is an important supplement. Lysozyme maintains its structure after being adsorbed on the $MoS_2$ surface in the 100 ns MD simulations, which may reflect the early stages of adsorption behaviors. The longer simulations and the improvement of simulation methodologies in the future will promote the better understanding of the adsorption process as Szleifer *et al.*[48] reminded in their work. These findings shed light on the molecular-level interaction mechanisms between proteins and an $MoS_2$ surface and provide useful information for the applications of $MoS_2$ in bio-related fields.

## ACKNOWLEDGMENTS

The authors acknowledge financial support from the National Natural Science Foundation of China (Nos. 21376089 and 91334202), the National Key Basic Research Program of China (No. 2013CB733500), Guangdong Science Foundation (2014A030312007), and the Fundamental Research Funds for the Central Universities (SCUT-2015ZP033). CPU hours allocated by the SCUTGrid at the South China University of Technology and the ScGrid of the Supercomputing Centre, Computer Network Information Centre of the Chinese Academy of Sciences are also gratefully acknowledged.

[1]K. S. Novoselov, A. K. Geim, S. V. Morozov, D. Jiang, Y. Zhang, S. V. Dubonos, I. V. Grigorieva, and A. A. Firsov, Science **306**, 666 (2004).
[2]A. H. Castro Neto, F. Guinea, N. M. R. Peres, K. S. Novoselov, and A. K. Geim, Rev. Mod. Phys. **81**, 109 (2009).
[3]Q. H. Wang, K. Kalantar-Zadeh, A. Kis, J. N. Coleman, and M. S. Strano, Nat. Nanotechnol. **7**, 699 (2012).
[4]M. Xu, T. Liang, M. Shi, and H. Chen, Chem. Rev. **113**, 3766 (2013).
[5]K. F. Mak, C. Lee, J. Hone, J. Shan, and T. F. Heinz, Phys. Rev. Lett. **105**, 136805 (2010).
[6]W. Z. Teo, E. L. K. Chng, Z. Sofer, and M. Pumera, Chem. Eur. J. **20**, 9627 (2014).
[7]C. N. Rao, K. Gopalakrishnan, and U. Maitra, ACS Appl. Mater. Interfaces **7**, 7809 (2015).
[8]K. Kalantar-zadeh and J. Z. Ou, ACS Sens. **1**, 5 (2016).
[9]B. L. Li, J. Wang, H. L. Zou, S. Garaj, C. T. Lim, J. Xie, N. B. Li, and D. T. Leong, Adv. Funct. Mater. **26**, 7034 (2016).
[10]W. L. Deblina Sarkar, X. Xie, A. C. Anselmo, S. Mitragotri, and K. Banerjee, ACS Nano **8**, 3992 (2014).
[11]L. Wang, Y. Wang, J. I. Wong, T. Palacios, J. Kong, and H. Y. Yang, Small **10**, 1101 (2014).
[12]C. H. Naylor, N. J. Kybert, C. Schneier, J. Xi, G. Romero, J. G. Saven, R. Liu, and A. T. C. Johnson, ACS Nano **10**, 6173 (2016).
[13]R. A. Latour, Biointerphases **3**, FC2 (2008).
[14]M. Ozboyaci, D. B. Kokh, S. Corni, and R. C. Wade, Q. Rev. Biophys. **49**, e4 (2016).
[15]H. Heinz and H. Ramezani-Dakhel, Chem. Soc. Rev. **45**, 412 (2016).
[16]Z. Gu, W. Li, L. Hong, and R. Zhou, J. Chem. Phys. **144**, 175103 (2016).
[17]Y. Ling, Z. Gu, S. G. Kang, J. Luo, and R. Zhou, J. Phys. Chem. C **120**, 6796 (2016).
[18]Z. Gu, Z. Yang, S. G. Kang, J. R. Yang, J. Luo, and R. Zhou, Sci. Rep. **6**, 28252 (2016).
[19]Z. Gu, P. De Luna, Z. Yang, and R. Zhou, Phys. Chem. Chem. Phys. **19**, 3039 (2017).
[20]V. Varshney, S. S. Patnaik, C. Muratore, A. K. Roy, A. A. Voevodin, and B. L. Farmer, Comput. Mater. Sci. **48**, 101 (2010).
[21]B. Luan and R. Zhou, Appl. Phys. Lett. **108**, 131601 (2016).
[22]A. P. Gaur, S. Sahoo, M. Ahmadi, S. P. Dash, M. J. Guinel, and R. S. Katiyar, Nano Lett. **14**, 4314 (2014).
[23]J. Zhou, S. Chen, and S. Jiang, Langmuir **19**, 3472 (2003).
[24]K. P. Fears, B. Sivaraman, G. L. Powell, Y. Wu, and R. A. Latour, Langmuir **25**, 9319 (2009).
[25]E. T. Harrison, T. Weidner, D. G. Castner, and G. Interlandi, Biointerphases **12**, 02D401 (2016).
[26]C. Peng, J. Liu, D. Zhao, and J. Zhou, Langmuir **30**, 11401 (2014).
[27]D. Zhao, C. Peng, and J. Zhou, Phys. Chem. Chem. Phys. **17**, 840 (2015).
[28]K. Kubiak-Ossowska and P. A. Mulheran, Langmuir **26**, 15954 (2010).
[29]G. Raffaini and F. Ganazzoli, Langmuir **26**, 5679 (2010).
[30]T. Wei, M. A. Carignano, and I. Szleifer, J. Phys. Chem. B **116**, 10189 (2012).
[31]Y. Xie, J. Zhou, and S. Jiang, J. Chem. Phys. **132**, 065101 (2010).
[32]N. Hildebrand, S. Köppen, L. Derr, K. Li, M. Koleini, K. Rezwan, and L. Colombi Ciacchi, J. Phys. Chem. C **119**, 7295 (2015).
[33]G. Yu, J. Liu, and J. Zhou, AIChE J. **61**, 2035 (2015).
[34]J. A. Kelly, A. R. Sielecki, B. D. Sykes, M. N. James, and D. C. Phillips, Nature **282**, 875 (1979).
[35]M. Calvaresi, S. Hoefinger, and F. Zerbetto, Chem. Eur. J. **18**, 4308 (2012).
[36]E. F. Pettersen, T. D. Goddard, C. C. Huang, G. S. Couch, D. M. Greenblatt, E. C. Meng, and T. E. Ferrin, J. Comput. Chem. **25**, 1605 (2004).
[37]D. B. A. D. MacKerell *et al.*, J. Phys. Chem. B **102**, 3586 (1998).
[38]W. L. Jorgensen, J. Chandrasekhar, J. D. Madura, R. W. Impey, and M. L. Klein, J. Chem. Phys. **79**, 926 (1983).
[39]C. K. B. Hess, D. van der Spoel, and E. Lindahl, J. Chem. Theory Comput. **4**, 435 (2008).
[40]W. Humphrey, A. Dalke, and K. Schulten, J. Mol. Graphics **14**, 33 (1996).
[41]S. Nosé, J. Chem. Phys. **81**, 511 (1984).

[42]B. Hess, H. Bekker, H. J. C. Berendsen, and J. G. E. M. Fraaije, J. Comput. Chem. **18**, 1463 (1997).
[43]T. Darden, D. York, and L. Pedersen, J. Chem. Phys. **98**, 10089 (1993).
[44]C. Peng, J. Liu, and J. Zhou, J. Phys. Chem. C **119**, 20773 (2015).
[45]W. Beckner, Y. He, and J. Pfaendtner, J. Phys. Chem. B **120**, 10423 (2016).
[46]P. A. Mulheran, D. J. Connell, and K. Kubiak-Ossowska, RSC Adv. **6**, 73709 (2016).
[47]C. Mucksch and H. M. Urbassek, J. Phys. Chem. B **120**, 7889 (2016).
[48]T. Wei, M. A. Carignano, and I. Szleifer, Langmuir **27**, 12074 (2011).